Chinese Journal of Natural Medicines

Total glucosides of paeony alleviates cGAS–STING–mediated diseases by blocking the STING–IRF3 interaction

Ye XIU, Sihao WANG, Ping ZHANG, Chengwei LI, Zhixin WU, Jincai WEN, Yingjie XU, Guiji LV, Xiaomei ZHAO, Xu DONG, Yichong CHEN, Junjie LI, Yan WANG, Liang ZOU, Xiaohe XIAO, Zhaofang BAI

Citation: Ye XIU, Sihao WANG, Ping ZHANG, Chengwei LI, Zhixin WU, Jincai WEN, Yingjie XU, Guiji LV, Xiaomei ZHAO, Xu DONG, Yichong CHEN, Junjie LI, Yan WANG, Liang ZOU, Xiaohe XIAO, Zhaofang BAI, Total glucosides of paeony alleviates cGAS–STING–mediated diseases by blocking the STING–IRF3 interaction, Chinese Journal of Natural Medicines, 2024, 22(5), 402–415. doi: 10.1016/S1875–5364(24)60572–8.

View online: https://doi.org/10.1016/S1875–5364(24)60572–8

Available online at www.sciencedirect.com
ScienceDirect
Chinese Journal of Natural Medicines 2024, **22**(5): 402-415
doi: 10.1016/S1875-5364(24)60572-8
Chinese Journal of Natural Medicines

•Original article•

Total glucosides of paeony alleviates cGAS-STING-mediated diseases by blocking the STING-IRF3 interaction

XIU Ye[1, 2, 3Δ], WANG Sihao[2, 3Δ], ZHANG Ping[4Δ], LI Chengwei[1, 2, 3], WU Zhixin[2, 3], WEN Jincai[2, 3], XU Yingjie[2, 3], LV Guiji[2, 3], ZHAO Xiaomei[2, 3], DONG Xu[2, 3], CHEN Yichong[1], LI Junjie[2, 3], WANG Yan[2, 3], ZOU Liang[5*], XIAO Xiaohe[1, 2, 3, 6*], BAI Zhaofang[1, 2, 3, 6*]

[1] *School of Pharmacy, Fujian University of Traditional Chinese Medicine, Fuzhou 350122, China;*
[2] *Department of Hepatology, The Fifth Medical Center of PLA General Hospital, Beijing 100039, China;*
[3] *China Military Institute of Chinese Materia, Fifth Medical Center of Chinese PLA General Hospital, Beijing 100039, China;*
[4] *Department of Pharmacy, Medical Supplies Center of PLA General Hospital, Beijing 100039, China;*
[5] *School of Food and Biological Engineering, Chengdu University, Chengdu 610106, China;*
[6] *National Key Laboratory of Kidney Diseases, Chinese PLA General Hospital, Beijing 100039, China*

Available online 20 May, 2024

[ABSTRACT] In the realm of autoimmune and inflammatory diseases, the cyclic GMP-AMP synthase (cGAS) stimulator of interferon genes (STING) signaling pathway has been thoroughly investigated and established. Despite this, the clinical approval of drugs targeting the cGAS-STING pathway has been limited. The Total glucosides of paeony (TGP) is highly anti-inflammatory and is commonly used in the treatment of rheumatoid arthritis (RA), emerged as a subject of our study. We found that the TGP markedly reduced the activation of the cGAS-STING signaling pathway, triggered by various cGAS-STING agonists, in mouse bone marrow-derived macrophages (BMDMs) and Tohoku Hospital Pediatrics-1 (THP-1) cells. This inhibition was noted alongside the suppression of interferon regulatory factor 3 (IRF3) phosphorylation and the expression of interferon-beta (IFN-β), C-X-C motif chemokine ligand 10 (CXCL10), and inflammatory mediators such as tumor necrosis factor-alpha (TNF-α) and interleukin-6 (IL-6). The mechanism of action appeared to involve the TGP's attenuation of the STING-IRF3 interaction, without affecting STING oligomerization, thereby inhibiting the activation of downstream signaling pathways. *In vivo*, the TGP hindered the initiation of the cGAS-STING pathway by the STING agonist dimethylxanthenone-4-acetic acid (DMXAA) and exhibited promising therapeutic effects in a model of acute liver injury induced by lipopolysaccharide (LPS) and D-galactosamine (D-GalN). Our findings underscore the potential of the TGP as an effective inhibitor of the cGAS-STING pathway, offering a new treatment avenue for inflammatory and autoimmune diseases mediated by this pathway.

[KEY WORDS] Total glucosides of gaeony; cGAS-STING pathway; Inflammation; LPS/D-GalN; STING inhibitor
[CLC Number] R965 **[Document code]** A **[Article ID]** 2095-6975(2024)05-0402-14

Introduction

The cyclic GMP-AMP synthase (cGAS) stimulator of interferon genes (STING) pathway, a pivotal component of the innate immune system's threat detection mechanism, has garnered significant global attention in recent years [1, 2]. Accumulating evidence indicates that the cGAS-STING pathway is implicated in the regulation of inflammation, autoimmune diseases, and antitumor immunity, extending beyond its established role in the innate immune response to microbial invasion [1, 3, 4]. The cytosolic DNA sensor cGAS catalyzes the conversion of ATP and GTP into the unconventional cyclic dinucleotide (CDN) c[G(2′, 5′)pA(3′, 5′)p], also known as 2′3′-cGAMP. This CDN, along with bacterial CDNs such as c-di-GMP and c-di-AMP, binds to and activates the endoplasmic reticulum (ER)-associated stimulator of STING. Upon activation, STING translocates from the ER to perinuclear vesicles through the Golgi apparatus. The recruitment and activation

[Received on] 20-Nov.-2023
[Research funding] This work was supported by the Natural Science Foundation of Beijing (No. 7232321), the Cultivating and Improving the Service Ability of Traditional Chinese Medicine (No. 2021ZY038), the Innovation Team and Talents Cultivation Program of National Administration of Traditional Chinese Medicine (No. ZYYCXTD-C-202005), the State Key Program of National Natural Science of China (Nos. 81930110, 82230118).
[*]**Corresponding author]** E-mails: zouliangcdu@126.com (ZOU Liang); pharmacy_302@126.com (XIAO Xiaohe); baizf2008@hotmail.com (BAI Zhaofang)
[Δ]These authors contributed equally to this work.
These authors have no conflict of interest to declare.

of Tank-binding kinase 1 (TBK1) by STING subsequently occurs, leading to the phosphorylation of IRF3. Activated IRF3 then dimerizes and enters the nucleus, effectively initiating the expression of IFN [5-7]. Additionally, the activation of STING triggers nuclear factor-kappa B (NF-κB) signaling *via* TBK1 and tumor necrosis factor receptor-associated factor 6 (TRAF6), culminating in the release of pro-inflammatory cytokines such as tumor necrosis factor-alpha (TNF-α) and interleukin-6 (IL-6) [8, 9]. Thus, the cGAS-STING pathway is crucial in fortifying the host immune system against microbial threats.

However, the hyperactivation of the cGAS-STING pathway can precipitate a variety of autoimmune and inflammatory conditions [10]. STING-associated vasculopathy with onset in infancy (SAVI) is an example of such a condition, manifesting as a systemic inflammatory disease characterized by vasculitis and pulmonary fibrosis, associated with increased functional mutations in the STING gene [5, 11]. Individuals afflicted with systemic autoimmune diseases, such as systemic lupus erythematosus (SLE), Sjögren's syndrome (SS), scleroderma, and dermatomyositis, exhibit prolonged upregulation of IFN expression. This elevated type I IFN expression is conclusively linked to the activation of the cGAS-STING pathway [12, 13]. In animal studies, hepatitis B virus (HBV) has been shown to evade immune detection by suppressing cGAS-STING expression and signaling [14]. Mice deficient in functional cGAS or STING exhibit significant resistance to myocardial infarction, suggesting a protective role against this severe cardiovascular disease [15]. Activation of the cGAS-STING pathway was also observed in lupus-prone TREX1-D18N mutants and Fcgr2b knockout mice, indicating its involvement in these autoimmune models [16, 17]. Additionally, exposure to lipopolysaccharide (LPS) and D-galactosamine (D-GalN) has been identified as a trigger for the release of mitochondrial DNA (mtDNA) into the cytosol, leading to excessive activation of the cGAS signaling cascade. This aberrant activation results in hepatocyte death and, ultimately, acute liver failure [18, 19]. LPS is known to increase the release of pro-inflammatory cytokines and the production of reactive oxygen species (ROS), while D-GalN impairs RNA metabolism in hepatocytes, contributing to liver damage [20]. Despite the discovery of numerous STING inhibitors in recent years, only a limited number of these agents have reached clinical use for the prevention and treatment of inflammatory and autoimmune diseases related to the cGAS-STING pathway.

In 1998, the China Food and Drug Administration granted approval for the Total glucosides of paeony (TGP) capsule to be marketed for the treatment of rheumatoid arthritis (RA) following clinical trials [21]. Additionally, TGP has been recommended for managing various autoimmune disorders, including SLE, SS, psoriasis, diabetes, diabetic nephropathy, ankylosing spondylitis, and immunological liver injury, among others. Recent studies have further highlighted the TGP's impact on several inflammation-associated signaling pathways, notably the NF-κB and PI3K/Akt pathways [21, 22]. This evidence led to speculation regarding the TGP's potential effects on the cGAS-STING pathway and, by extension, its influence on autoimmunity and inflammatory diseases associated with this pathway, necessitating further investigation.

In our study, we identified that the TGP might act as an inhibitor of the cGAS-STING signaling pathway. Specifically, the TGP inhibits the STING-IRF3 interaction, thus preventing the activation of the cGAS-STING pathway. Notably, it does not interfere with STING oligomerization or the interactions between STING-TBK1 or TBK1-IRF3. Moreover, the TGP demonstrated effective therapeutic outcomes in models induced by the STING agonist dimethylxanthenone-4-acetic acid (DMXAA) and in models of acute liver injury (ALI) induced by LPS and D-GalN. Consequently, we propose that the TGP may offer therapeutic benefits for autoimmune and inflammatory diseases associated with the cGAS-STING pathway. This novel insight holds potential for further clinical validation and application.

Materials and Methods

Animals

C57BL/6 mice aged 6−8 weeks and weighing 18−22 g were obtained from the Beijing Specific Pathogen-Free (SPF) Biotechnology Company Limited. These mice were acclimatized for one week in a sterile laboratory environment designed for mice, under a 12-hour light-dark cycle. They had access to clean drinking water and were provided with fresh mouse food daily. The room temperature was maintained at 25 ± 2°C. The Animal Health Committee of the Fifth Medical Center of the Chinese General Hospital of the People's Liberation Army granted approval for all the animal experimental studies conducted.

Cell culture

Bone marrow-derived macrophages (BMDMs) were isolated from the femurs of an 8-week-old female C57BL/6 mouse and cultured in Dulbecco's Modified Eagle Medium (DMEM). Tohoku Hospital Pediatrics-1 (THP-1) human leukemia monocytes were maintained in Roswell Park Memorial Institute (RPMI) 1640 medium, while human embryonic kidney (HEK-293T) cells were grown in DMEM. All culture media were supplemented with 10% fetal bovine serum (FBS) and 1% penicillin-streptomycin. The incubation conditions for all cell types were set at 37 °C with a 5% CO_2 atmosphere.

Reagents and antibodies

Opti-MEM (2427634) and Penicillin-Streptomycin (CC004) were sourced from Macgene (Beijing, China). DMEM (PYG0073) and RPMI 1640 (PYG0006) were acquired from BOSTER (Wuhan, China), while Fetal Bovine Serum (FBS) was purchased from VivaCell (Shanghai, China). Murine macrophage colony-stimulating factor (M-CSF), 2'3'-cGAMP (HY-100564), Vadimezan (DMXAA) (HY-10964), diABZI STING agonist-1 trihydrochloride (diABZI) (HY-112921B), Phorbol 12-myristate 13-acetate

(PMA) (HY-18739), and H-151 (HY-112693) were all procured from Med Chem Express (Shanghai, China). DMSO (D2650) and LPS (12880) were obtained from Sigma-Aldrich (St. Louis, MO, USA), and DMXAA (DM0234) from Chengdu Durst Biotechnology Co., Ltd. (Chengdu, China). D-GalN (G8110) came from Solarbio (Beijing, China). The Protease Inhibitors Cocktail (C0001) was supplied by TargetMol (Shanghai, China), and the Color Prestained Protein Marker by Vazyme (Beijing, China).

Rabbit monoclonal anti-Phospho-IRF-3 antibody (1 : 2000, 86691) was supplied by Gene Tex (Texas, USA). Polyclonal antibodies for TMEM173/STING (1 : 3000, 19851-1-AP), IRF3 (1 : 5000, 11312-1-AP), and HSP90 (1 : 5000, 13171-1-AP), along with Anti-DDDK tag (1 : 5000, 0543-1-AP) and HA tag polyclonal antibodies (1 : 5000, 51064-2-AP), were provided by Proteintech Group (Chicago, USA).

Equimolar amounts of sense and antisense DNA oligonucleotides were annealed at 95 °C for 10 min and then allowed to cool to room temperature to synthesize interferon stimulatory DNA (ISD) at a concentration of 1.375 mg·mL^{-1}. The sequences of the DNA oligonucleotides used are provided in Table 1.

Table 1 DNA oligonucleotides sequences

Target gene	Sequence (5′-3′)
ISD	TACAGATCTACTAGTGATCTATGACTGATCTGTACATGATCTACA
	TGTAGATCATGTACAGATCAGTCATAGATCACTAGTAGATCTGTA

Quality control of the TGP Capsule

The TGP Capsule (220420) was purchased from Ningbo Liwah Pharmaceutical Co., Ltd. (Ningbo, China). Chromatographic analyses were performed using an Agilent ZORBAX RRHD SB-C_{18} column (2.1 mm × 50 mm, 1.8 μm). The mobile phases consisted of 0.1% phosphoric acid. The injection volume was set at 5 μL, with a flow rate of 0.2 mL·min^{-1}. The high-performance liquid chromatography (HPLC) chromatogram of TGP is depicted in Fig. 1. The principal components of TGP were identified by comparing the retention times of the chromatographic peaks with those of known chemical reference standards. A total of 10 peaks were observed in the chromatogram, with the fifth peak identified as Paeoniflorin (PA), comprising approximately 42% of the TGP composition based on external standardization of the peak area relative to the standard. The detailed results from the analysis of the TGP content are provided in Table 2.

BMDMs and THP-1 cells were seeded in 96-well plates at a concentration of 1.2 × 10^6 cells·mL^{-1}. Following overnight incubation at 37 °C, the supernatant was removed, and the cells were treated with media containing varying concentrations of TGP for an additional 12 h. To assess cell viability, cells were incubated for 1 h with a cell counting kit-8 (CCK-8) solution (Abbkine, KTC1020-10000T, Wuhan, China). The absorbance at 450 nm was measured using a Microplate Reader (SpectraMax Absorbance Reader CMax Plus, Molecular Devices, BioTek, USA). The effect of the drugs on cell viability was determined by analyzing the optical density (OD) values.

Western blotting assay

To assess the protein expression of p-IRF3, IRF3, and STING, we conducted Western blotting assay using HSP90

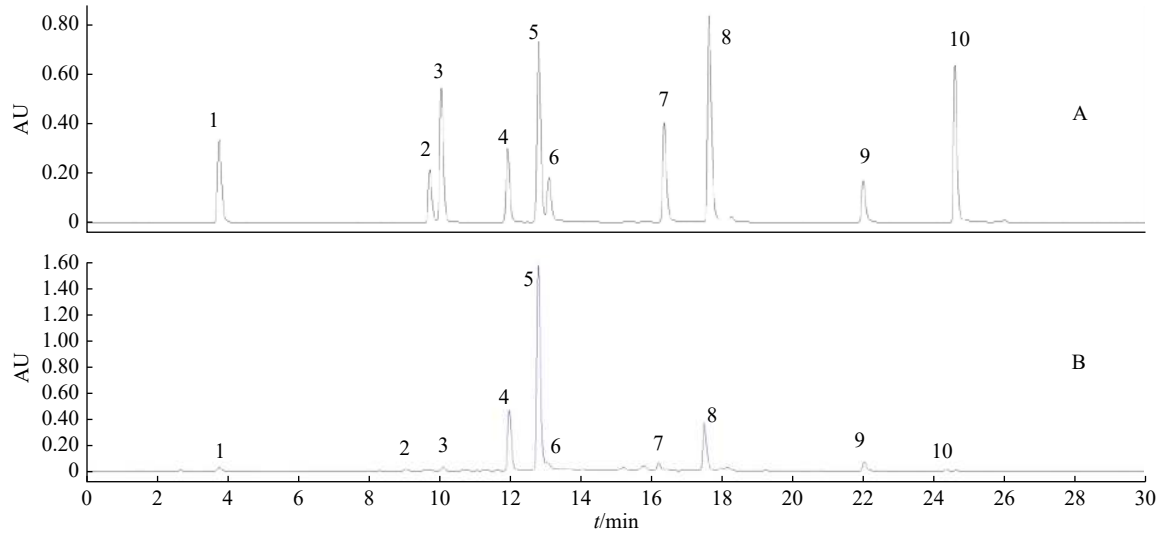

Fig. 1 HPLC analysis of the TGP Capsule. The chromatographic profile of TGP Capsule. The injection volume and the flow rate were 5 μL and 0.2 mL·min^{-1}. (A) Mixed standard of a reference substance. (B) TGP Capsule. Peak 1: Gallic acid, Peak 2: Oxypaeoniflorin, Peak 3: Catechin, Peak 4: Albiflorin, Peak 5: Paeoniflorin, Peak 6: Ethyl gallate, Peak 7: Galloyl paeoniflorin, Peak 8: 1,2,3,4,6-O-pentagalloylglucose, Peak 9: Benzoyloxypaeoniflorin, Peak 10: Benzoylpaeoniflorin

Table 2 TGP Capsule sample content measurement results (mg·g^{-1})

Serial number	Sample 1	Sample 2	Average value
Oxypaeoniflorin	1.99	2.07	2.0
Albiflorin	143.11	145.12	144.1
Paeoniflorin	420.17	424.03	422.1
Benzoylpaeoniflorin	2.27	2.30	2.3
1,2,3,4,6-*O*-pentagalloylglucose	103.32	100.33	101.8

as the loading control. Whole-cell lysates from BMDMs and THP-1 cells were prepared by gentle agitation in 1× RIPA buffer containing 50 mmol·L^{-1} Tris-HCl (pH 7.45), 150 mmol·L^{-1} NaCl, 1% Triton X-100, 1% sodium deoxycholate, and supplemented with5 × SDS-PAGE loading RIPA buffer. The protein samples were then heated at 105 °C for 15 min in a metal bath. After the protein samples were heated at 105 °C for 15 min in a metal bath, electrophoresis was conducted using 10% sodium dodecyl sulfate-polyacrylamide gel electrophoresis (SDS-PAGE). An equal volume of protein was loaded onto a 10% SDS-PAGE gel and initially ran at 75 V for 0.5 h. After the protein marker on the separation gel was pre-stained, the voltage was increased to 135 V, and the run continued for another hour. Following this, proteins were wet-transferred to a polyvinylidene fluoride (PVDF) membrane at 100 V for 1 h. The membrane was subsequently blocked with TBST containing 5% skim milk powder for 1 h. Overnight incubation at 4°C with the respective primary antibodies followed. The next day, after collecting the primary antibody, the membrane was washed thrice with TBST and then incubated with the corresponding secondary antibody at a dilution of 1 : 5000 for 1 h. Post-secondary antibody incubation, the membrane underwent three TBST washes. Protein expression levels were then visualized using a commercial enhanced chemiluminescence (ECL) kit following the manufacturer's instructions, and X-ray films were scanned using an Epson Perfection V800 photo scanner.

Enzyme-linked immunosorbent assay (ELISA)

Alanine aminotransferase (ALT) and aspartate aminotransferase (AST) levels in mouse serum were quantified using the methods outlined in the ALT and AST assay kits provided by Nanjing Jiancheng Bioengineering Institute (Nanjing, China). Additionally, the concentrations of TNF-α, IL-6, and IFN-β in mouse serum and peritoneal lavage fluid were measured following the protocols of the ELISA kits for TNF-α (1217202) and IL-6 (1210602) from Dakewe (Shenzhen, China), and for mouse IFN-β (EK2236) from Lianke (Hangzhou, China).

Quantitative real-time PCR (qRT-PCR)

Total RNA was isolated from cells and liver tissue using Trizol reagent (Alcatel, 111003, Genstar). This was followed by cDNA synthesis using the StarScript III All-in-one RT Mix reverse transcription reagent (A230-10, Genstar), performed in a gene amplifier (peqSTAR 2X, Peqlab, Germany). The synthesized cDNA was then combined with 2 × RealStar Fast SYBR Green Master Mix (A304-10, Genstar) as per the provided instructions. The relative expression levels of target genes were quantified using the $^{\Delta\Delta}$CT method on a QuantStudio 6 Real-Time PCR system (Gentier 96E, Xi'an, China). The sequences of the primers used are listed in Table 3.

Immunofluorescence

BMDMs and THP-1 cells were seeded into 96-well plates and incubated overnight. Following this, the supernatants were removed, and the cells were treated with a medium containing (200 μg·mL^{-1}) TGP for 1 h. Subsequently, di-ABZI was added to stimulate the cells for 2 h. After stimulation, the supernatants were discarded, and the cells were washed once with phosphate-buffered saline (PBS) before being fixed with 4% paraformaldehyde for 30 min. Following another PBS wash, cells were permeabilized with 0.25% Triton X-100 for 15 min. Cells were then blocked with a quick-sealing solution for 1 h at room temperature. Following the removal of the blocking solution, the cells were incubated overnight with an IRF3 antibody (1 : 100) or an anti-P65 antibody (1 : 100) at 4 °C. The next day, after removing the primary antibody and washing thrice with PBS, cells were incubated with Alexa Fluor® 488 conjugated goat anti-rabbit IgG antibody for 1 h at room temperature. Finally, the cells were stained with Hoechst (1 : 5000) for 15 min to visualize nuclei. Imaging was performed using a confocal microscope (FV3000, OLYMPUS).

Immunoprecipitation

HEK-293T cells were plated at a density of 5 × 10^5 cells·mL^{-1} in 6-well plates. Upon reaching full adherence, plasmids encoding Flag-TBK1, HA-STING, Flag-IRF3, and HA-IRF3 were mixed with transfection reagent and introduced into the cells for 18 h. Subsequently, cells were treated with TGP (200 μg·mL^{-1}) for 6 h. The supernatant was then removed, and cells were lysed with 600 μL of RIPA buffer (50 mmol·L^{-1} Tris-HCl, pH 7.4, 150 mmol·L^{-1} NaCl, 1% Triton X-100, 0.5% sodium deoxycholate) supplemented with 1% protease inhibitor cocktail for 15 min, followed by centrifugation at 4 °C and 12 000 r·min^{-1} for 15 min. A portion of the supernatant was directly mixed with 1 × and 5 × SDS-PAGE loading RIPA buffer. The remainder of the supernatant was incubated with anti-Flag M2 affinity beads at 4 °C for 4 h for immunoprecipitation. After centrifugation, the supernatant was discarded, leaving the anti-Flag M2 affinity beads, to which 100 μL of mixed 1 × and 5 × SDS-PAGE loading RIPA buffer was added. Both cell lysates and im-

Table 3 Quantitative PCR primer sequences

Target gene	Sequence (5′-3′)
Mouse *Actin*	GGCTGTATTCCCCTCCATCG
	CCAGTTGGTAACAATGCCATGT
Mouse *IFN-β*	TCCGAGCAGAGATCTTCAGGAA
	TGCAACCACCACTCATTCTGAG
Mouse *CXCL10*	ATCATCCCTGCGAGCCTATCCT
	GACCTTTTTTGGCTAAACGCTTTC
Mouse *ISG15*	GGTGTCCGTGACTAACTCCAT
	CTGTACCACTAGCATCACTGTG
Mouse *THF-α*	GGGCAGTTAGGCATGGGAT
	TGAGCCTTTTAGGCTTCCCAG
Mouse *IL-6*	CACTTCACAAGTCGGAGGCT
	CTGCAAGTGCATCATCGTTGT
Human *Actin*	CATGTACGTTGCTATCCAGGC
	CTCCTTAATGTCACGCACGAT
Human *IFN-β*	TCCAAATTGCTCTCCTGTTG
	GCAGTATTCAAGCCTCCCAT
Human *CXCL10*	TGGCATTCAAGGAGTACCTC
	TTGTAGCAATGATCTCAACACG
Human *THF-α*	CCTCTCTCTAATCAGCCCTCTG
	GAGGACCTGGGAGTAGATGAG
Human *IL-6*	ACTCACCTCTTCAGAACGAATTG
	CCATCTTTGGAAGGTTCAGGTTG

munoprecipitates were analyzed by Western blotting assay.

STING oligomerization assay

BMDMs were seeded in 12-well plates at a density of 1.2×10^6 cells·mL^{-1} and incubated overnight. The cells were then pre-treated with Opti-mem medium containing TGP (200 μg·mL^{-1}) for 1 h, followed by transfection with cGAMP for 30 min. After discarding the supernatant, cells were lysed with 400 μL of Triton buffer (50 mmol·L^{-1} Tris-HCl, 150 mmol·L^{-1} NaCl, 0.5% Triton X-100, pH 7.5, and 1% n-Dodecyl-β-D-maltoside) supplemented with 1% protease inhibitor cocktail. The lysate was centrifuged at 4 °C and 12,000 r·min^{-1} for 10 min. A portion of the supernatant was mixed with 1 × and 5 × SDS-PAGE loading RIPA buffer, and another portion was prepared for loading onto a native-PAGE gel using a native sample buffer. The native-PAGE gel was run in electrophoresis buffer (25 mmol·L^{-1} Tris-HCl, pH 8.4, and 192 mmol·L^{-1} glycine, with and without 1% deoxycholate in the cathode and anode chambers), followed by immersion of the gel in SDS electrophoresis buffer for 30 min. Subsequent steps were in accordance with Western blotting procedures.

Mice and animal experiment design

Mice were randomly allocated into seven groups (n = 6 per group): (1) control group, (2) LPS/D-GalN group, (3) TGP (100 mg·kg^{-1}) group, (4) TGP (200 mg·kg^{-1}) group, (5) LPS/D-GalN + TGP (100 mg·kg^{-1}), (6) LPS/D-GalN + TGP (200 mg·kg^{-1}), (7) LPS/D-GalN + H-151 (10 mg·kg^{-1}) group. To mitigate liver injury, mice in the TGP-treated groups received the respective dose of TGP *via* oral gavage daily for seven days prior to the experiment. Mice in both the control and LPS/D-GalN groups received an equivalent volume of normal saline. Concurrently with the final dose, mice in the positive control group received an intraperitoneal injection of H-151 (10 mg·kg^{-1}). One hour later, LPS (2.5 mg·kg^{-1}) and D-GalN (250 mg·kg^{-1}) were administered intraperitoneally to induce liver injury. Four hours post-induction, mice were anesthetized and euthanized, and their liver tissues were collected for hematoxylin and eosin (H&E) staining, TUNEL staining, mRNA analysis of relevant genes, and serum for ALT, AST, and cytokine ELISA assays.

Separately, eight-week-old female C57BL/6 mice were divided into three groups for the DMXAA *in vivo* assay. Mice in the TGP-treated group received TGP (200 mg·kg^{-1}) *via* oral gavage, while mice in the control and model groups were given an equal volume of saline daily for seven consecutive days. On the seventh day, one hour post-TGP administration, the control group was injected intraperitoneally with saline, and the model and TGP-treated groups with DMXAA (25 mg·kg^{-1}). Four hours later, mice were euthanized for the collection of serum and peritoneal lavage fluid, with subsequent ELISA measurements of IFN-β, TNF-α, and IL-6 levels in both samples.

Statistical analysis

Data analysis was conducted using GraphPad Prism 8 software. Comparisons between two groups were performed using unpaired Student's *t*-tests, while comparisons among multiple groups were conducted using one-way ANOVAs followed by Dunnett's post hoc tests. *P*-values less than 0.05 were considered statistically significant. All experimental results were presented as mean ± standard error of the mean (SEM).

Results

TGP inhibits DNA-triggered activation of the cGAS-STING signaling pathway in BMDMs and THP-1 cells

The inappropriate activation of the cGAS-STING signaling pathway, triggered by cytoplasmic DNA anomalies, has recently been implicated in autoimmune diseases and inflammation, drawing considerable attention [23, 24]. To assess potential drug toxicity, we first examined the cellular viability of TGP in BMDMs and THP-1 cells. Before evaluating cell viability, BMDMs and THP-1 cells were treated with various concentrations of TGP for 12 h. The results indicated that TGP did not exhibit significant cytotoxicity in BMDMs and THP-1 cells, even at the highest concentration tested (800 μg·mL^{-1}) (Fig. 2A). Following this, we explored the impact of TGP on the activation of the cGAS-STING signaling pathway in BMDMs, stimulated by ISD. Western blotting analys-

is revealed that TGP inhibited the ISD-induced phosphorylation of IRF3 in a dose-dependent manner (Fig. 2B). Concurrently, we quantified the mRNA levels of IFN-β, CXCL10, TNF-α, and IL-6 using qPCR. These analyses showed that TGP significantly attenuated the increases in IFN-β, CXCL10, TNF-α, and IL-6 mRNA levels induced by ISD stimulation (Figs. 2D−2G). To ascertain whether TGP exerts a similar inhibitory effect on human cell lines, we assessed its impact on the cGAS-STING pathway in THP-1 cells. The results confirmed that TGP also dose-dependently reduced IRF3 phosphorylation in ISD-stimulated THP-1 cells (Fig. 2C). Moreover, TGP effectively prevented the rise in IFN-β, CXCL10, and the pro-inflammatory mediators TNF-α and IL-6 in response to ISD stimulation (Figs. 2H−2K). Consequently, these findings suggest that TGP suppresses the activation of the cGAS-STING pathway triggered by cytosolic DNA (e.g., ISD) in both BMDMs and THP-1 cells.

TGP significantly inhibits signal transduction dependent on various canonical STING stimulators

Our research then focused on assessing how TGP modulates the activation of the cGAS-STING pathway in response to various established STING stimulators, aiming to evaluate TGP's potential as a broad-spectrum inhibitor of this pathway. Classical STING stimulators such as exogenous cGAMP, which activates the cGAS-STING pathway *via* 2,3-cGAMP, and DMXAA and diABZI, which stimulate the pathway by directly targeting STING, were examined [25, 26]. Western blotting analysis showed that TGP decreased the phosphorylation of IRF3 caused by ISD, cGAMP, diABZI, and DMXAA in BMDMs but had no impact on the levels of IRF3 and STING (Fig. 3A). Correspondingly, qPCR assays demonstrated that TGP significantly lowered the mRNA expressions of *IFN-β*, *CXCL10*, and the inflammatory mediators *TNF-α* and *IL-6* in BMDMs, induced by these STING activators (Figs. 3C−3F). The same inhibitory effect of TGP on STING agonist-induced signal transduction was confirmed in THP-1 cells, a human monocytic cell line, as shown by similar reductions in IRF3 phosphorylation and mRNA levels of *IFN-β*, *CXCL10*, *TNF-α*, and *IL-6* (Figs. 3B, 3G−3J). These findings suggest that TGP effectively impedes the signal transduction induced by multiple STING agonists in both BMDMs and THP-1 cells.

TGP disrupted the interaction of STING-IRF3 but had no effect on STING oligomerization

Upon activation by its agonists, STING transitions from the endoplasmic reticulum to the Golgi apparatus, recruiting and activating TBK1, which then phosphorylates IRF3. This phosphorylated IRF3 undergoes dimerization and nuclear translocation, leading to the production of IFNs. Additionally, activation of the cGAS-STING pathway promotes NF-κB-mediated transcriptional activation, highlighting its importance in immune response regulation [27, 28]. To assess the impact of TGP on this pathway, we first examined its effect on the nuclear translocation of IRF3. Immunofluorescence assays revealed that TGP significantly inhibited the nuclear translocation of p65 in BMDMs and IRF3 in THP-1 cells induced by diABZI (Figs. 4A and 4B). Given that cGAMP binds to STING, facilitating its translocation to the Golgi apparatus and subsequent recruitment of TBK1 and IRF3, the phosphorylation of IRF3 by TBK1, followed by its dimerization and nuclear translocation, is a key mechanism in signal transduction, particularly in controlling IFN expression. This process involves the formation of a trimeric STING-TBK1-IRF3 complex [29]. Our findings demonstrated that TGP hindered the interaction of STING with IRF3 but had no effect on the interactions of STING-TBK1 and TBK1-IRF3 (Figs. 4C−4E). Considering the essential role of STING oligomerization, triggered by cGAMP binding to STING dimers on the ER membrane, in activating downstream signaling, we also investigated the effect of TGP on STING oligomerization. Our findings showed that TGP does not influence the oligomerization of STING in BMDMs (Fig. 4F). These outcomes suggest that TGP may inhibit the activation of the cGAS-STING pathway by specifically blocking the interaction between STING and IRF3.

TGP inhibits DMXAA-induced activation of STING and downstream signaling in vivo

We furtherly chose an agonist of STING, DMXAA, to examine if TGP affected the cGAS-STING pathway *in vivo*. DMXAA is an agonist for murine STING, and it can induce strong pro-inflammatory responses both *in vitro* and *in vivo*. It binds to murine STING in a way similar to that of the endogenous agonis and activates the TBK1-IRF3 axis to induce potent IFN-β production [30]. In addition, engagement of STING by DMXAA also activates the canonical and the non-canonical NF-κB pathways and thereby induces the expression of pro-inflammatory cytokines. To determine whether TGP prevented STING from being activated in mice, and then influenced the production of downstream genes, mice in this study were dosed continuously for seven days and DMXAA was injected intraperitoneally 1 h after the last dose. Mouse serum and intraperitoneal lavage fluid were gathered and the concentrations of IFN-β, TNF-α, and IL-6 in these samples were measured. We found that TGP reduced the level of DMXAA-induced IFN-β and elevated the expression of inflammatory mediators TNF-α and IL-6. (Figs. 5A−5F). Through agonist models induced by DMXAA, we found that TGP significantly inhibited DMXAA-induced IFN-β production and downstream signaling inflammatory factor release *in vivo*.

TGP reduces LPS/D-GalN-induced acute liver damage by preventing the cGAS-STING signaling pathway from being activated.

According to previous studies, LPS/D-GalN dramatically increases mtDNA release in the cytoplasm *in vivo*. This promotes an excessive amount of cGAS signaling, which causes liver cell death, liver damage, and other negative effects [19]. Considering these findings, we have opted for the LPS/D-GalN-induced acute ALI model to probe the potential inhibitory effects of TGP upon the activation of the cGAS-

STING signaling cascade *in vivo*. H-151 is a potent STING inhibitor with significant inhibitory activity *in vitro* and *in vivo*, which can inhibit STING palmitoylation and block TBK1 phosphorylation [31, 32]. To determine whether TGP reduces inflammation and liver damage brought on by LPS/D-GalN by blocking the cGAS-STING pathway, we used H-151 as a positive control in this experiment. The liver in the LPS/D-GalN group significantly increased local cell death, inflammatory cell infiltration, and partial bleeding when compared to the normal group, while the TGP administration group significantly reduced these inflammatory and bleeding reactions. The H&E staining was used to examine the pathological changes in the liver tissue (Fig. 6A). TUNEL staining revealed that there were less TUNEL-positive hepatocytes in the group that received TGP treatment than there were in the group that received LPS/D-GalN (Fig. 6B). Furthermore, it was shown that the increase in ALT and AST in the LPS/D-GalN group could be inhibited by the TGP dosage group in a dose-dependent way (Figs. 6C and 6D). At the same time, it was found by ELISA reagent detection that the mice in the

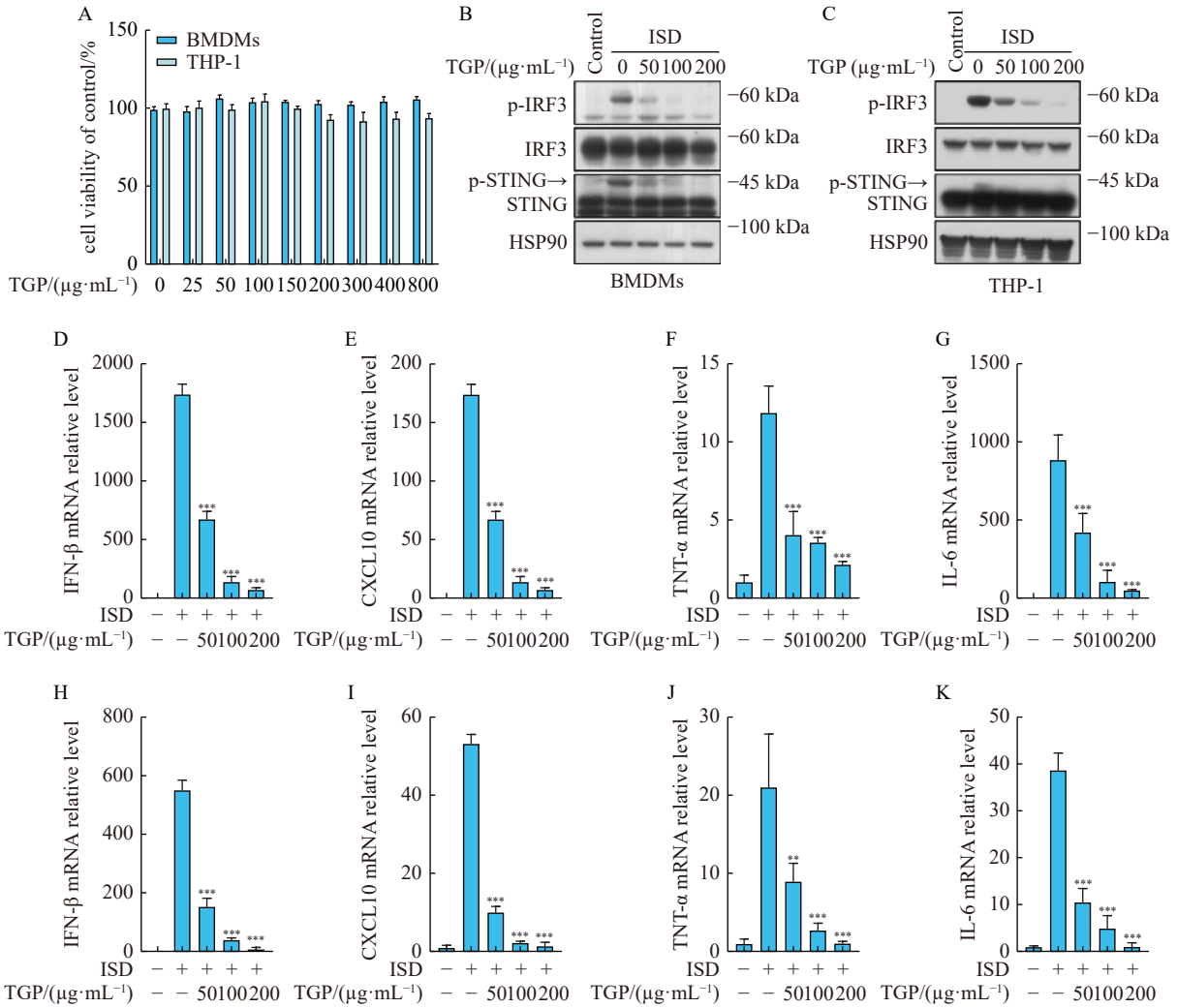

Fig. 2 TGP inhibits DNA-triggered activation of the cGAS-STING signaling pathway in BMDMs and THP-1 cells. (A) The CCK-8 was used to determine the vitality of BMDMs and THP-1 cells after being exposed to different dosages of TGP over a period of 12 h. (B, C) Prior to the transfection of ISD (2.5 μg·mL^{-1}) stimulation for a duration of 1.5 h, BMDMs and THP-1 cells were subjected to a 1 h pretreatment with diverse concentrations of TGP. Subsequently, the expression levels of p-IRF3, STING, IRF3, and HSP90 were meticulously scrutinized through the employment of Western blotting analysis. (D−G) BMDMs were pre-treated with distinct concentrations of TGP for 1 h, after which they were stimulated with ISD (2.5 μg·mL^{-1}) for a duration of 4 h. QPCR was conducted to measure the subsequent expression levels of IFN-β, CXCL10, TNF-α, and IL-6 mRNA. (H−K) Similarly, THP-1 cells were also pre-treated with various concentrations of TGP for 1 h before being subjected to ISD (2.5 μg·mL^{-1}) stimulation for a period of 4 h. After that, the mRNA expression levels of IFN-β, CXCL10, TNF-α, and IL-6 were assessed by qPCR. One-way ANOVA was used to evaluate statistical differences together with Dunnett's post hoc test. Information about the data: The error bars show the mean ± SEM of three technical replicates ($n = 6$). $^{*}P < 0.05$, $^{**}P < 0.01$, $^{***}P < 0.001$ *vs* LPS/D-GalN group.

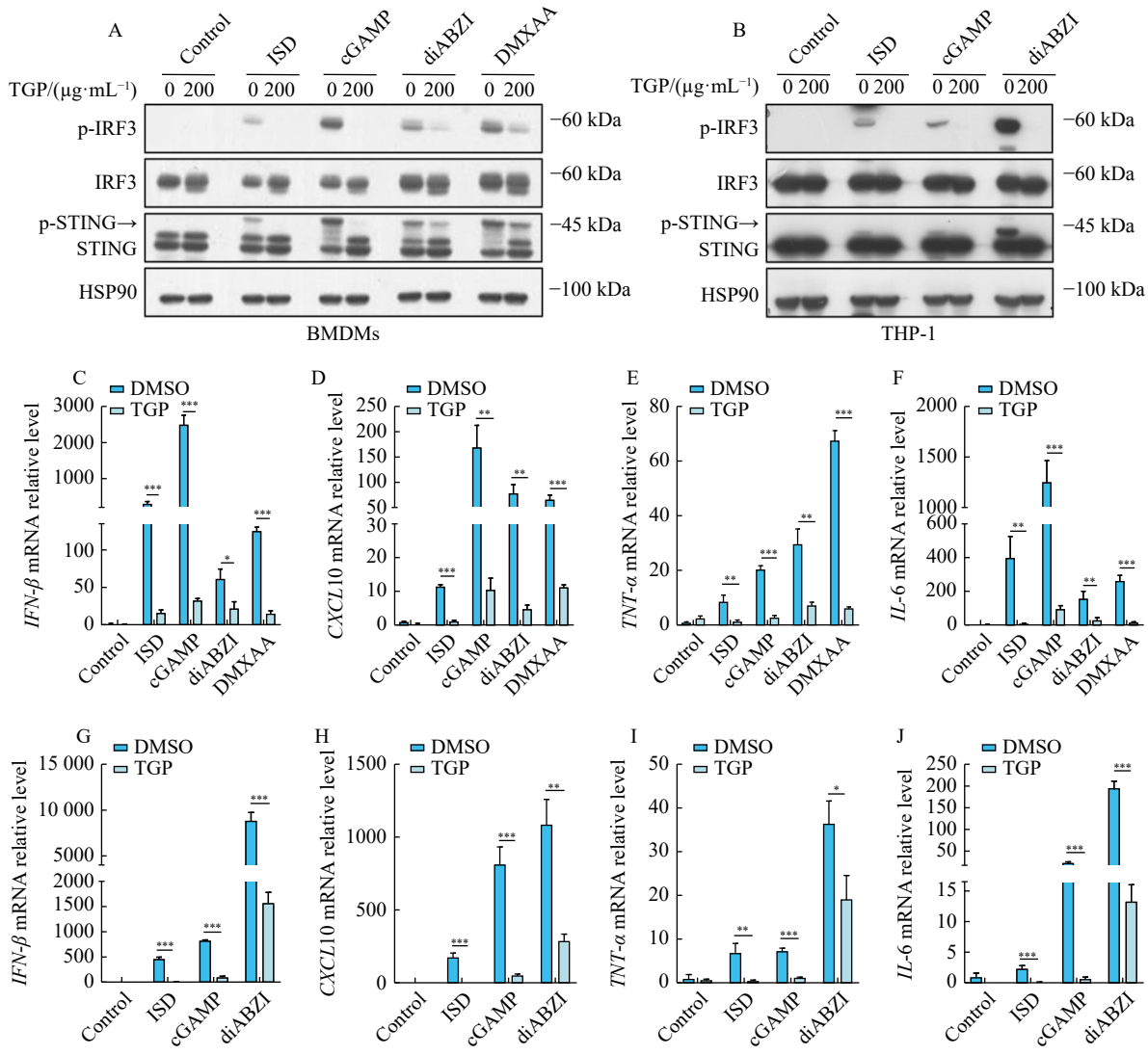

Fig. 3 TGP significantly inhibits signal transduction dependent on various canonical STING stimulators. (A) BMDMs were firstly incubated with TGP (200 μg·mL^{-1}) for 1 h, subsequently stimulated with ISD (2.5 μg·mL^{-1}), cGAMP (2.5 μg·mL^{-1}), diABZI (10 μmol·L^{-1}), and DMXAA (12.5 μg·mL^{-1}) for 1.5 h. P-IRF3, STING, and IRF3 expressions in whole-cell lysates were assessed by immunoblotting analysis. (B) THP-1 cells were pre-treated with TGP (200 μg·mL^{-1}) for 1 h, followed by stimulation with ISD (2.5 μg·mL^{-1}), cGAMP (2.5 μg·mL^{-1}), and diABZI (10 μmol·L^{-1}) for 1.5 h. Immunoblotting was utilized to assess p-IRF3, STING, and IRF3 expression in whole cell lysates. (C, D, E, F) BMDMs were pre-incubated with TGP (200 μg·mL^{-1}) for 1 h, thereafter stimulated with ISD, cGAMP, diABZI, and DMXAA for 4 h. Subsequently, qPCR was employed to detect the mRNA expression levels of *IFN-β*, *CXCL10*, *TNF-α*, and *IL-6*. (G, H, I, J) THP-1 cells were pre-treated with TGP (200 μg·mL^{-1}) for 1 h, followed by stimulation with ISD, cGAMP, and diABZI for 4 h. Thereafter, qPCR analysis was employed to determine the mRNA expression levels of *IFN-β*, *CXCL10*, *TNF-α*, and *IL-6*. Data information: The three technical replicates' mean ± SEM (n = 3) is represented by the error bars. The unpaired *t*-test was used to evaluate statistical differences, with $^{*}P < 0.05$, $^{**}P < 0.01$, $^{***}P < 0.001$ *vs* DMSO Group .

TGP administration group expressed relative lower levels of IFN-β factor and related inflammatory factors TNF-α and IL-6 compared to the mice in the LPS/D-GalN group (Figs. 6E−6G). In addition, we employed qPCR to identify IFN-β and associated downstream genes as well as the expression of inflammatory markers in liver tissue to investigate whether TGP inhibits the cGAS-STING pathway to minimize LPS/D-GalN-induced inflammation and liver injury. The findings demonstrated that TGP significantly reduced the levels of IFN-β, CXCL10, interferon-stimulated gene 15 (ISG15), TNF-α and IL-6 mRNA (Figs. 6H−6L).

Furthermore, compared to the LPS/D-GalN group, the extent of liver injury was markedly mitigated following H-151 treatment, characterized by reduced inflammatory cell infiltration and improved hemorrhagic conditions (Figs. 6A and 6B). The administration of H-151 successfully lowered serum levels of ALT and AST, along with the levels of pro-inflammatory cytokines IFN-β, TNF-α, and IL-6, relative to the

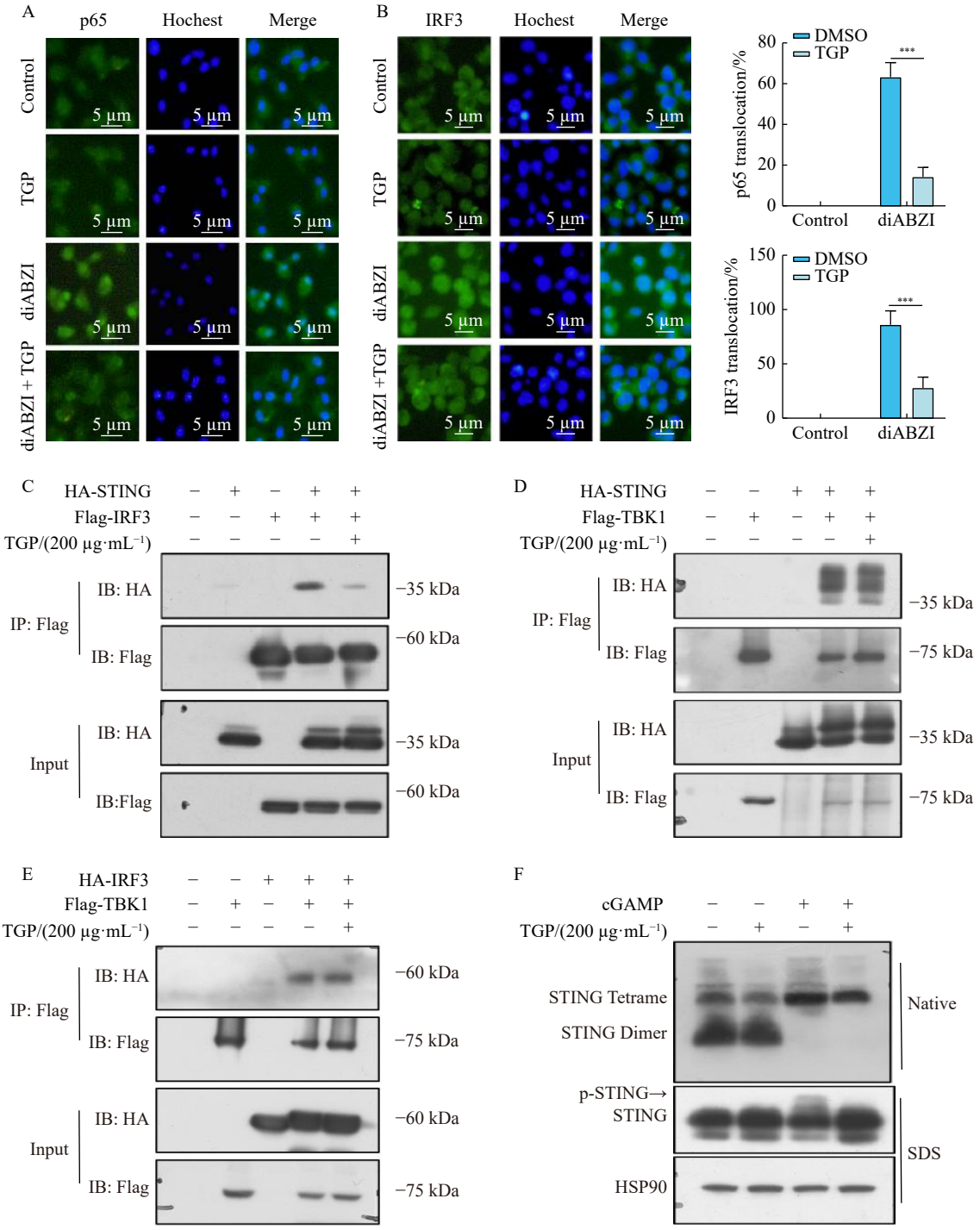

Fig. 4 TGP disrupted the interaction of STING-IRF3, but has no effect on STING oligomerization. (A) BMDMs are pre-treated with TGP (200 μg·mL^{-1}) for 1 h, then stimulated with diABZI for 2 h, Subsequently, immunostaining was performed using anti-p65 antibodies, and the resulting images were captured (Scale bars, 5 μm). (B) THP-1 are pre-treated with TGP (200 μg·mL^{-1}) for 1 h, then stimulated with diABZI for 2 h. Immunostaining was then conducted using anti-IRF3 antibodies, and the resulting images were captured (Scale bars, 5 μm). (C) HEK-293T cells were subjected to 6 h treatment with TGP (200 μg·mL^{-1}). Investigation of the interaction between Flag-IRF3 and HA-STING by immunoprecipitation. (D) HEK-293T cells were subjected to 6 h treatment with TGP (200 μg·mL^{-1}). Investigation of the interaction between Flag-TBK1 and HA-STING by immunoprecipitation. (E) HEK-293T cells were subjected to 6 h treatment with TGP (200 μg·mL^{-1}). Investigation of the interaction between Flag-TBK1 and HA-IRF3 by immunoprecipitation. (F) BMDMs were stimulated with cGAMP for 0.5 h after a 1 h pre-incubation with TGP (200 μg·mL^{-1}). Immunoblotting analysis was performed to assess the oligomerization and phosphorylation of STING. One-way ANOVA was used to evaluate statistical differences together with the Dunnett's post hoc test. Information about the data: The error bars show the mean ± SEM of three technical replicates. $^{*}P < 0.05$, $^{**}P < 0.01$, $^{***}P < 0.001$ *vs* DMSO group.

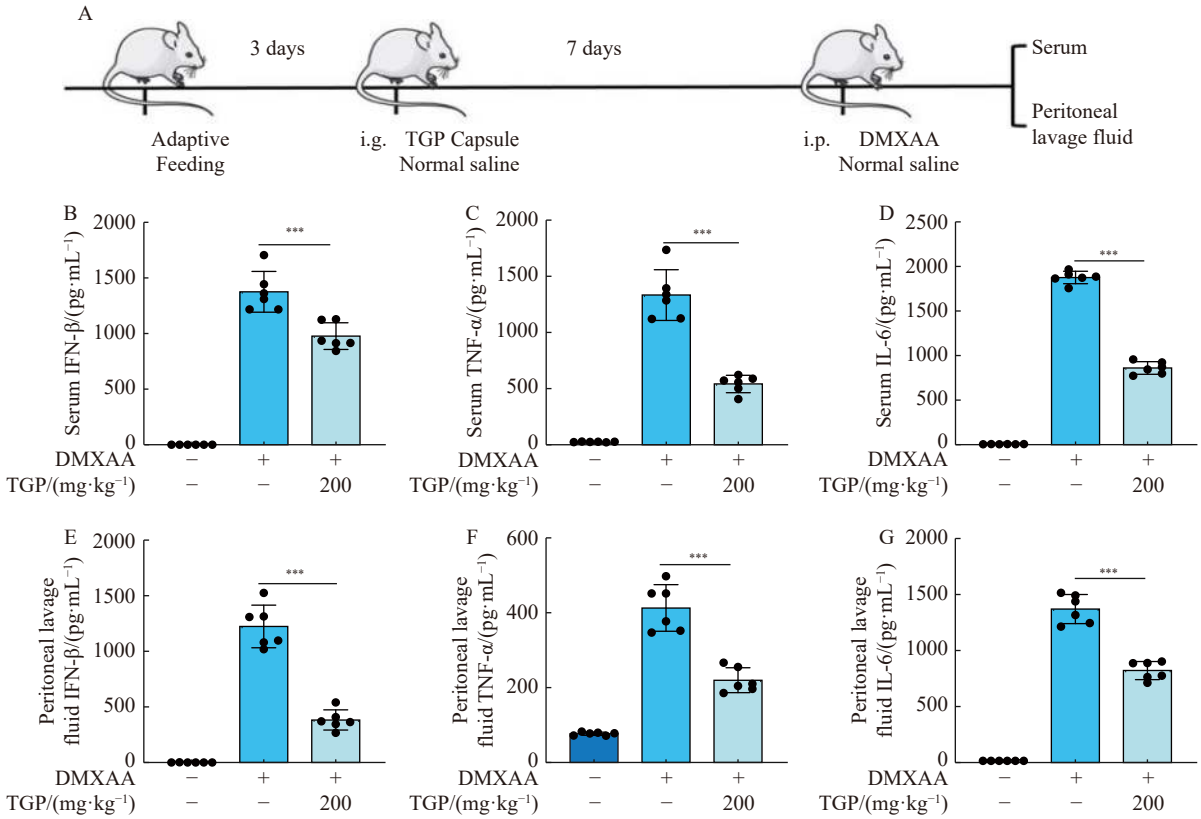

Fig. 5 TGP inhibits DMXAA-induced activation of STING and downstream signaling *in vivo* (A) The protocol of DMXAA-induced mice model. (B–G) 8-week-old female C57BL/6 mice were injected with saline or TGP (200 mg·kg^{-1}, i.g.) as pretreatment for seven days. On the last day, DMXAA (25 mg·kg^{-1}) (n = 6) was injected intraperitoneally 1 h after the administration of TGP. Serum and intraperitoneal lavage fluid were obtained 4 h later. The levels of IFN-β, TNF-α and IL-6 in serum and intraperitoneal lavage fluid were determined by enzyme-linked immunosorbent assay. One-way ANOVA was used to evaluate statistical differences together with the Dunnett's post hoc test. Information about the data: The error bars show the mean ± SEM of six technical replicates. $^{*}P < 0.05$, $^{**}P < 0.01$, $^{***}P < 0.001$ *vs* DMXAA group.

model group (Figs. 6C–6G). Quantitative PCR (qPCR) was utilized to measure the expression of *IFN-β* mRNA, *CXCL10* mRNA, *ISG15* mRNA, *TNF-α mRNA*, and *IL-6 mRNA* in the liver tissues of the H-151 treated group. As anticipated, the expression of these genes was significantly diminished after H-151 treatment (Figs. 6H–6L). In summary, TGP effectively reduced the surge of inflammatory markers in LPS/D-GalN-induced ALI and suppressed the expression of genes associated with the cGAS-STING pathway, thereby significantly alleviating liver injury in mice (Fig. 7). Given these experimental outcomes and the pivotal role of the cGAS-STING system in mediating inflammatory responses, it is proposed that TGP may exert therapeutic effects on LPS/D-GalN-induced ALI by obstructing the cGAS-STING pathway and curtailing the expression of inflammatory mediators.

Discussion

In recent years, a growing body of research has established that aberrant activation of the cGAS-STING signaling pathway is central to the development of autoimmune and inflammatory diseases. The innate immune system serves as the primary defense mechanism against potential threats, responding to a variety of stimuli, including exogenous pathogen-associated molecular patterns (PAMPs) and endogenous damage-associated molecular patterns (DAMPs). These threats are recognized by various pattern recognition receptors (PRRs), such as cGAS, leading to the activation of the immune response characterized by the release of IFN and numerous pro-inflammatory cytokines, which can precipitate inflammatory and autoimmune diseases [33, 34]. STING, an essential adaptor within host cells, plays a crucial role in this process by mediating signals from cGAMP, enabling the detection of both exogenous and endogenous DNA fragments by cGAS, and triggering innate immune responses. Over the past decades, the incidence of inflammatory diseases has been rising steadily, presenting a significant public health challenge and a threat to human well-being. Consequently, there is a pressing need to discover compounds that can effectively inhibit the cGAS-STING signaling pathway, offering potential therapeutic strategies for managing inflammatory and autoimmune diseases.

The TGP capsule, officially approved for the treatment of RA in 1998, is a classical Chinese patent medicine renowned for its anti-inflammatory and immunomodulatory effects. The primary active ingredient in the TGP is derived from the roots of Paeoniae Radix Alba (PRA), with TGP pre-

dominantly comprising monoterpenoid glycosides such as PA, albiflorin, benzoylpaeoniflorin, and oxypaeoniflorin. These compounds constitute the pharmacological foundation of peony's therapeutic benefits [21, 35]. Natural products have played a significant role in the prevention and treatment of inflammatory diseases, with compounds like quercetin, icariin, artemisinin, and triptolide contributing to this legacy [36]. As a natural compound, PA has been extensively utilized in the management of various inflammatory and liver conditions, including cholestatic liver injury, ALI, non-alcoholic fatty liver disease, liver fibrosis, and liver cancer, demonstrating its wide applicability and potential for clinical use [37]. Previous research has highlighted PA's promising prospects as a patent medicine. Although the TGP has been shown to possess liver-protective properties, there has yet to be research elucidating its effects on ALI from the perspective of innate immunity.

To our knowledge, this study marks the first demonstration of the impact of the TGP on the activation of the cGAS-STING signaling pathway. Initial investigations using cellular models revealed that the TGP had no discernible effect on the oligomerization of STING, a critical step in the initiation of the signaling cascade that follows the binding of cGAMP to STING dimers on the ER membrane. This finding suggested that the TGP's site of action might be downstream in the pathway. After moving through the ER-Golgi intermediate compartment (ERGIC) and the Golgi apparatus, STING recruits TBK1, facilitating TBK1 autophosphorylation. This leads to the formation of a trimeric complex with IRF3, STING, and TBK1, where TBK1 phosphorylates IRF3. Consequently, IRF3 is able to homodimerize and then translocate into the nucleus, thereby regulating gene expression. The formation of the STING-TBK1-IRF3 trimeric complex is essential for TBK1 activation and downstream IRF3 signaling[29]. Our findings indicate that the TGP specifically inhibits the interaction between STING and IRF3 rather than

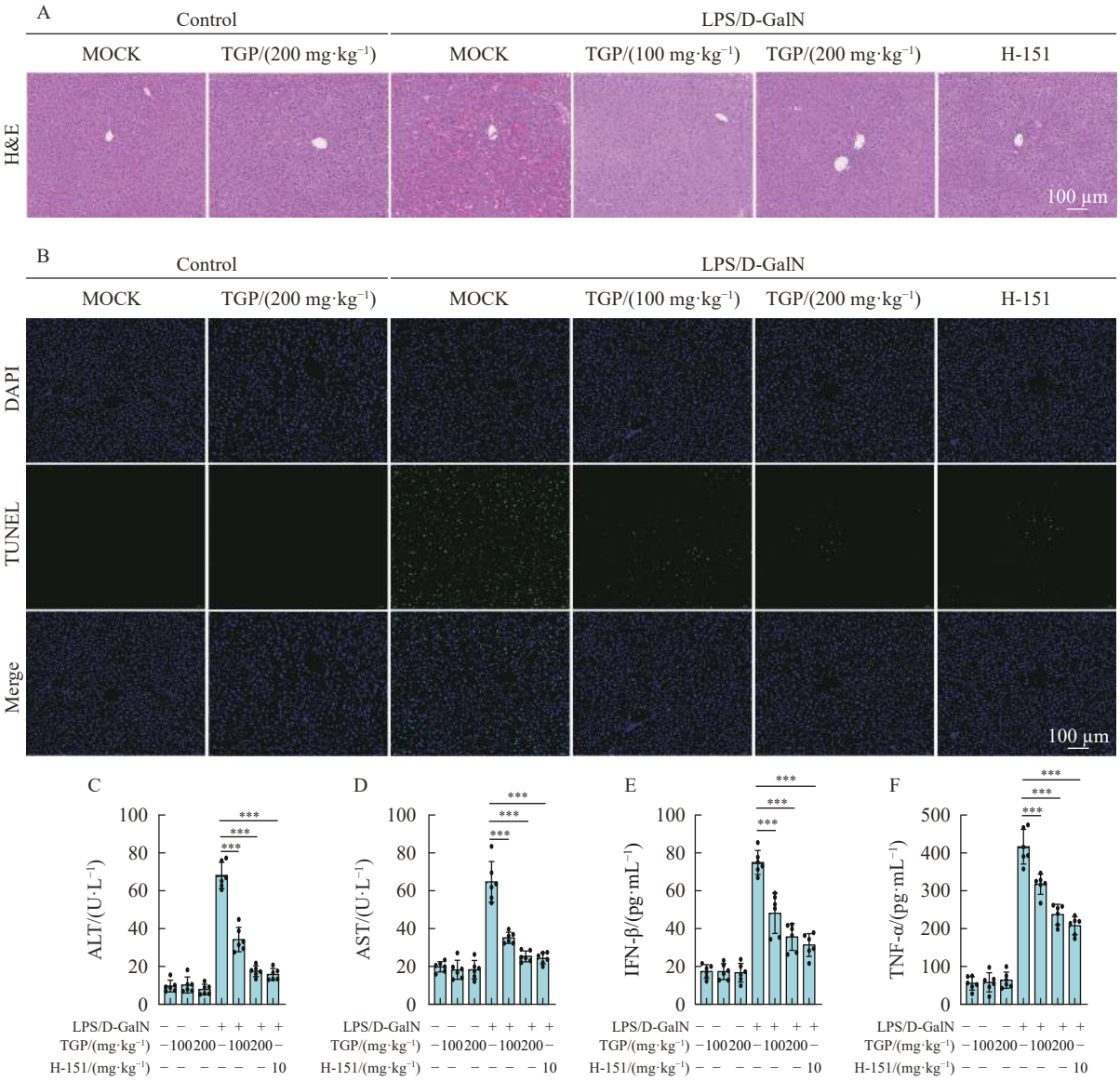

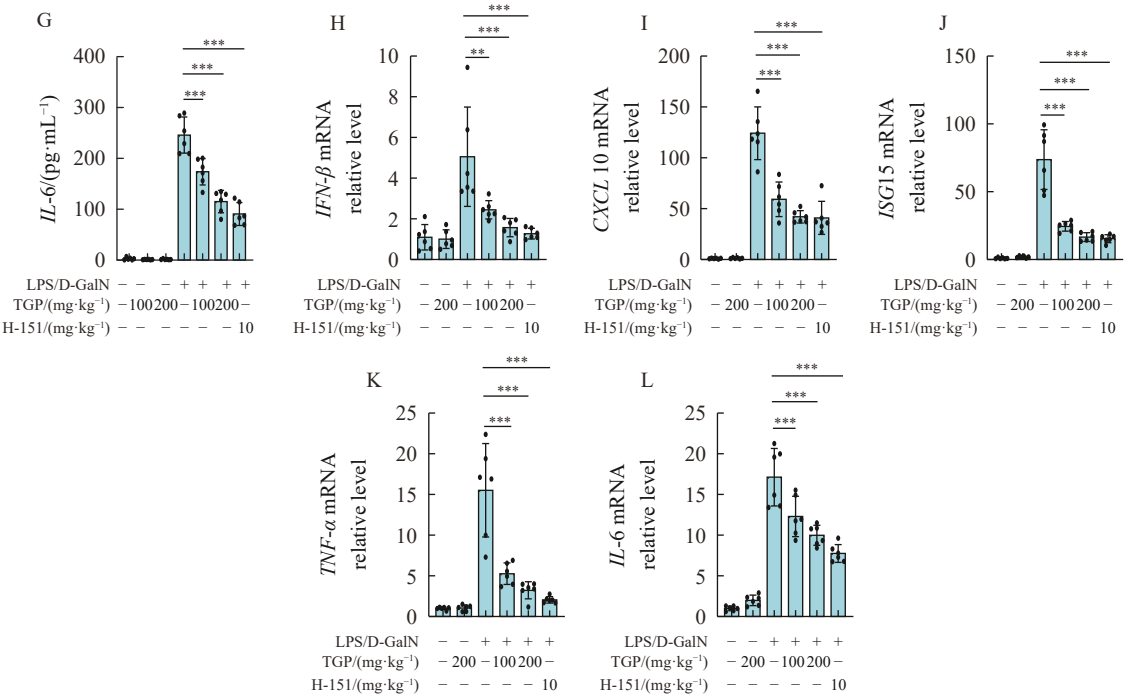

Fig. 6 TGP reduces LPS/D-GalN-induced acute liver damage by preventing the cGAS-STING signaling pathway from being activated. 8 weeks old female C57BL/6 mice were continuously administrated TGP at concentration of 100 or 200 mg·kg^{-1} for seven days under the same growth conditions. After 1 h at last time administration of TGP, mice were injected intraperitoneally with LPS/D-GalN (2.5 mg·kg^{-1} of LPS and 250 mg·kg^{-1} of D-GalN) for 4 h. Meanwhile, another group of mice were injected intraperitoneally with H-151 (10 mg·kg^{-1}) for 1h and then injected intraperitoneally with LPS/D-GalN for 4 h. (n = 6 per group). (A) Histological pictures of liver tissue sections stained with H&E 20 × (scale bar = 100 μm) are displayed. (B) Representative images of TUNEL staining (original magnification 20 × , scale bar = 100 μm). (C−G) Using ELISA, the levels of IFN-β, TNF-α, and IL-6 as well as the serum concentrations of ALT and AST (n = 6 per group) were assessed. (H−L) qPCR analysis was used to detect the mRNA levels of *IFN-β*, *CXCL10*, *ISG15*, *TNF-α* and *IL-6* (n = 6 per group). One-way ANOVA was used to evaluate statistical differences together with the Dunnett's post hoc test. Information about the data: The error bars show the mean ± SEM of six technical replicates. $^{*}P < 0.05$, $^{**}P < 0.01$, $^{***}P < 0.001$ *vs* LPS/D-GalN group.

affecting the binding of STING to TBK1 or TBK1 to IRF3. This insight advances our understanding of how the TGP acts to prevent activation of the cGAS-STING pathway, shedding light on the intrinsic mechanisms involved.

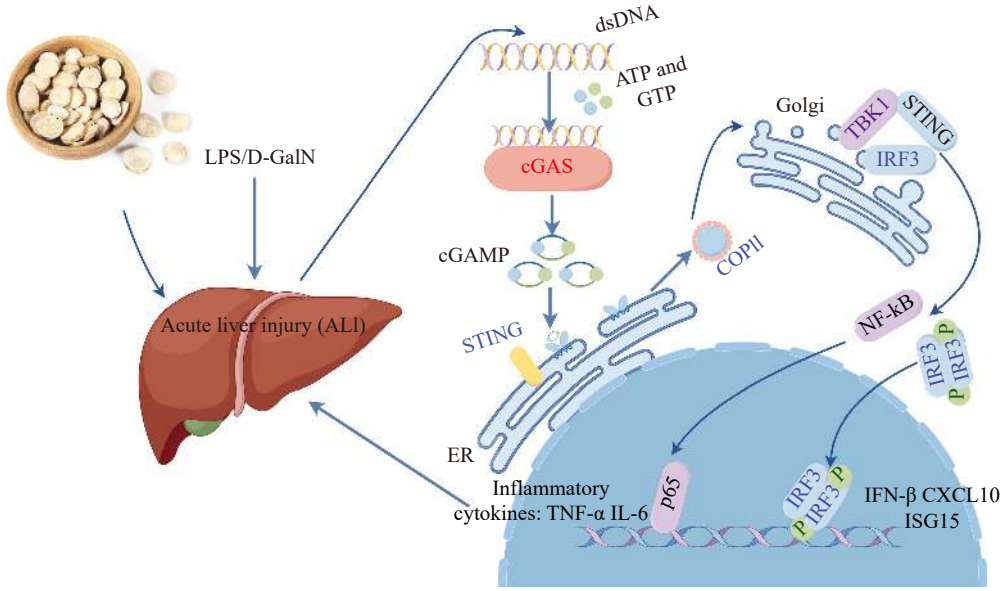

Fig. 7 TGP alleviates LPS/D-GalN-induced ALI by inhibiting the cGAS-STING signaling pathway.

In an agonist model induced by DMXAA that specifically stimulates STING, we observed a reduced production of IFN-β, TNF-α, and IL-6 following the administration of the TGP. Furthermore, employing a severe liver injury model caused by LPS and D-GalN, we concluded that the TGP possesses anti-inflammatory and anti-autoimmune properties through the cGAS-STING pathway. Our results showed that the administration of the TGP mitigated liver injury and suppressed the release of IFNs and pro-inflammatory cytokines.

The TGP has demonstrated therapeutic effects comparable to H-151, a potent inhibitor of the STING pathway, both *in vitro* and *in vivo*, as highlighted by our findings. The search for effective inhibitors of the cGAS-STING pathway has garnered global interest due to its significant role in the development of autoimmune and inflammatory diseases. Among the identified inhibitors targeting the STING pathway are compounds such as H-151, C-178, C-176, and nitro-fatty acids (NO_2-FAs), which inhibit STING by targeting its palmitoylation site [38, 39], Additionally, cyclic di-GMP (c-di-GMP) can competitively inhibit cGAMP-induced STING activation, producing a STING conformation distinct from that induced by cGAMP [1, 39, 40]. However, research into STING inhibitors is still at an early stage, with no candidates having advanced to clinical trials yet. In our study, H-151 was used as a positive control to compare the effects of the TGP on the cGAS-STING pathway. Our results showed that administration of the TGP effectively prevented the release of TNF-α, IL-6, and IFN-β to a similar extent as H-151, along with the amelioration of liver injury as evidenced by the reduction in ALT and AST levels. From these findings, we concluded that the TGP may modulate the cGAS-STING pathway, impacting autoimmunity and inflammatory diseases. This significant discovery provides practical evidence supporting the use of officially approved drugs in clinical trials for treating diseases associated with the cGAS-STING pathway.

In this study, we delineated how TGP suppressed the cGAS-STING pathway both *in vivo* and *in vitro*, leading to the conclusion that the TGP represents a promising inhibitor of this signaling pathway. Particularly noteworthy is our exploration within a cGAS-STING-mediated disease model, specifically acute liver damage induced by LPS/D-GalN, where we concluded that TGP could be an ideal choice for treatment strategies targeting autoimmunity and inflammatory diseases. This finding introduces a novel approach for clinical practice in managing autoimmune and inflammatory conditions triggered by the cGAS-STING signaling pathway, providing a valuable insight into potential therapeutic avenues.

References

[1] Decout A, Katz JD, Venkatraman S, *et al*. The cGAS-STING pathway as a therapeutic target in inflammatory diseases [J]. *Nat Rev Immunol*, 2021, **21**(9): 548-569.

[2] Zhang X, Bai XC, Chen ZJ. Structures and mechanisms in the cGAS-STING innate immunity pathway [J]. *Immunity*, 2020, **53**(1): 43-53.

[3] Du H, Xu T, Cui M. cGAS-STING signaling in cancer immunity and immunotherapy [J]. *Biomed Pharmacother*, 2021, **133**: 110972.

[4] Gan Y, Li X, Han S, *et al*. The cGAS/STING pathway: a novel target for cancer therapy [J]. *Front Immunol*, 2021, **12**: 795401.

[5] Hong Z, Mei J, Li C, *et al*. STING inhibitors target the cyclic dinucleotide binding pocket [J]. *Proc Natl Acad Sci U S A*, 2021, **118**(24): e2105465118.

[6] Wen J, Qin S, Li Y, *et al*. Flavonoids derived from licorice suppress LPS-induced acute lung injury in mice by inhibiting the cGAS-STING signaling pathway [J]. *Food Chem Toxicol*, 2023, **175**: 113732.

[7] Luo W, Xu G, Song Z, *et al*. Licorice extract inhibits the cGAS-STING pathway and protects against non-alcoholic steatohepatitis [J]. *Front Pharmacol*, 2023, **14**: 1160445.

[8] Hopfner KP, Hornung V. Molecular mechanisms and cellular functions of cGAS-STING signalling [J]. *Nat Rev Mol Cell Biol*, 2020, **21**(9): 501-521.

[9] Zhang L, Wei X, Wang Z, *et al*. NF-κB activation enhances STING signaling by altering microtubule-mediated STING trafficking [J]. *Cell Rep*, 2023, **42**(3): 112185.

[10] Skopelja-Gardner S, An J, Elkon KB. Role of the cGAS-STING pathway in systemic and organ-specific diseases [J]. *Nat Rev Nephrol*, 2022, **18**(9): 558-572.

[11] Frémond ML, Hadchouel A, Berteloot L, *et al*. Overview of STING-associated vasculopathy with onset in infancy (SAVI) among 21 patients [J]. *J Allergy Clin Immunol Pract*, 2021, **9**(2): 803-818.e811.

[12] Barrat FJ, Crow MK, vashkiv LB. Interferon target-gene expression and epigenomic signatures in health and disease [J]. *Nat Immunol*, 2019, **20**(12): 1574-1583.

[13] Barrera MJ, Aguilera S, Castro I, *et al*. Dysfunctional mitochondria as critical players in the inflammation of autoimmune diseases: potential role in Sjögren's syndrome [J]. *Autoimmun Rev*, 2021, **20**(8): 102867.

[14] Verrier ER, Yim SA, Heydmann L, *et al*. Hepatitis B virus evasion from cyclic guanosine monophosphate-adenosine monophosphate synthase sensing in human hepatocytes [J]. *Hepatology*, 2018, **68**(5): 1695-1709.

[15] King KR, Aguirre AD, Ye YX, *et al*. IRF3 and type I interferons fuel a fatal response to myocardial infarction [J]. *Nat Med*, 2017, **23**(12): 1481-1487.

[16] Xiao N, Wei J, Xu S, *et al*. cGAS activation causes lupus-like autoimmune disorders in a TREX1 mutant mouse model [J]. *J Autoimmun*, 2019, **100**: 84-94.

[17] Thim-Uam A, Prabakaran T, Tansakul M, *et al*. Erratum: STING mediates lupus *via* the activation of conventional dendritic cell maturation and plasmacytoid dendritic cell differentiation [J]. *iScience*, 2020, **23**(11): 101706.

[18] Chen R, Du J, Zhu H, *et al*. The role of cGAS-STING signalling in liver diseases [J]. *JHEP Rep*, 2021, **3**(5): 100324.

[19] Li J, Lu Y, Lin G. Blocking cGAS/STING signaling protects against sepsis-associated acute liver injury [J]. *Int Immunopharmacol*, 2022, **113**(Pt A): 109276.

[20] Yang W, Wang Y, Zhang C, *et al*. Maresin1 protect against ferroptosis-induced liver injury through ROS inhibition and Nrf2/HO-1/GPX4 activation [J]. *Front Pharmacol*, 2022, **13**: 865689.

[21] Jiang H, Li J, Wang L, *et al*. Total glucosides of paeony: a review of its phytochemistry, role in autoimmune diseases, and mechanisms of action [J]. *J Ethnopharmacol*, 2020, **258**: 112913.

[22] Zhang L, Wei W. Anti-inflammatory and immunoregulatory effects of paeoniflorin and total glucosides of paeony [J]. *Pharmacol Ther*, 2020, **207**: 107452.

[23] Hu MM, Shu HB. Innate immune response to cytoplasmic DNA: mechanisms and diseases [J]. *Annu Rev Immunol*, 2020, **38**: 79-98.

[24] Chen Q, Sun L, Chen ZJ. Regulation and function of the cGAS-

STING pathway of cytosolic DNA sensing [J]. *Nat Immunol*, 2016, **17**(10): 1142-1149.
[25] Ramanjulu JM, Pesiridis GS, Yang J, *et al*. Design of amidobenzimidazole STING receptor agonists with systemic activity [J]. *Nature*, 2018, **564**(7736): 439-443.
[26] Ding C, Song Z, Shen A, *et al*. Small molecules targeting the innate immune cGAS–STING–TBK1 signaling pathway [J]. *Acta Pharm Sin B*, 2020, **10**(12): 2272-2298.
[27] Dou Z, Ghosh K, Vizioli MG, *et al*. Cytoplasmic chromatin triggers inflammation in senescence and cancer [J]. *Nature*, 2017, **550**(7676): 402-406.
[28] Zhang C, Shang G, Gui X, *et al*. Structural basis of STING binding with and phosphorylation by TBK1 [J]. *Nature*, 2019, **567**(7748): 394-398.
[29] Ghosh M, Saha S, Bettke J, *et al*. Mutant p53 suppresses innate immune signaling to promote tumorigenesis [J]. *Cancer Cell*, 2021, **39**(4): 494-508.e495.
[30] Papinska J, Bagavant H, Gmyrek GB, *et al*. Activation of stimulator of interferon genes (STING) and Sjögren Syndrome [J]. *J Dent Res*, 2018, **97**(8): 893-900.
[31] Pan Y, You Y, Sun L, *et al*. The STING antagonist H-151 ameliorates psoriasis *via* suppression of STING/NF-κB-mediated inflammation [J]. *Br J Pharmacol*, 2021, **178**(24): 4907-4922.
[32] Hu S, Gao Y, Gao R, *et al*. The selective STING inhibitor H-151 preserves myocardial function and ameliorates cardiac fibrosis in murine myocardial infarction [J]. *Int Immunopharmacol*, 2022, **107**: 108658.
[33] Ablasser A, Chen ZJ. cGAS in action: expanding roles in immunity and inflammation [J]. *Science*, 2019, **363**(6431): eaat8657.
[34] Verrier ER, Langevin C. Cyclic guanosine monophosphate-adenosine monophosphate synthase (cGAS), a multifaceted platform of intracellular DNA sensing [J]. *Front Immunol*, 2021, **12**: 637399.
[35] Cao XY, Ni JH, Wang X, *et al*. Total glucosides of Paeony restores intestinal barrier function through inhibiting Lyn/Snail signaling pathway in colitis mice [J]. *Phytomedicine*, 2021, **87**: 153590.
[36] Zhu Y, Ouyang Z, Du H, *et al*. New opportunities and challenges of natural products research: when target identification meets single-cell multiomics [J]. *Acta Pharm Sin B*, 2022, **12**(11): 4011-4039.
[37] Ma X, Zhang W, Jiang Y, *et al*. Paeoniflorin, a natural product with multiple targets in liver diseases-a mini review [J]. *Front Pharmacol*, 2020, **11**: 531.
[38] Hansen AL, Buchan GJ, Rühl M, *et al*. Nitro-fatty acids are formed in response to virus infection and are potent inhibitors of STING palmitoylation and signaling [J]. *Proc Natl Acad Sci U S A*, 2018, **115**(33): E7768-E7775.
[39] Haag SM, Gulen MF, Reymond L, *et al*. Targeting STING with covalent small-molecule inhibitors [J]. *Nature*, 2018, **559**(7713): 269-273.
[40] Gong W, Lu L, Zhou Y, *et al*. The novel STING antagonist H151 ameliorates cisplatin-induced acute kidney injury and mitochondrial dysfunction [J]. *Am J Physiol Renal Physiol*, 2021, **320**(4): F608-F616.

Cite this article as: XIU Ye, WANG Sihao, ZHANG Ping, *et al*. Total glucosides of paeony alleviates cGAS-STING-mediated diseases by blocking the STING-IRF3 interaction [J]. *Chin J Nat Med*, 2024, **22**(5): 402-415.

Professor Liang Zou is the Director of the Science and Technology Department at Chengdu University.He is one of the leading scientists in the Molecular Pharmacology and Biopharmacy Laboratory at Chengdu University. He has been working in the field of naturally derived bioactives and nanomedicines for approximately 20 years, with his current research focusing on the pharmacological effects of active ingredients from Traditional Chinese Medicine.

Prof. Xiaohe Xiao is the director of Academic Committee of Senior Department of Hepatology of the Fifth Medical Center of Chinese PLA General Hospital, and director of China Military Institute of Chinese Materia Medica, with the professional and technical rank of Major General. He is the recipient of the National Science Fund for Distinguished Young Scholars, one of the first batch of National Qihuang Scholars, the National Ten Outstanding Youths of Traditional Chinese Medicine.

Prof. Bai Zhaofang is the director of the Institute of Department of Hepatology of the Fifth Medical Center of Chinese PLA General Hospital, the vice director of China Military Institute of Chinese Materia Medica, and reserve academic leader of National Key Discipline of clinical traditional Chinese pharmacy. He mainly engages in research on the immunopharmacology and immunotoxicology of Traditional Chinese Medicine.